



OPEN ACCESS

EDITED BY

Praveen Kumar Balachandran,
Vardhaman College of Engineering, India

REVIEWED BY

Sudhakar Babu Thanikanti,
Chaitanya Bharathi Institute of Technology,
India
Kasi Ramakrishnareddy Ch,
Vasavi College of Engineering, India
Pratikanta Mishra,
SRM University, India

*CORRESPONDENCE

Kareem M. AboRas,
✉ kareem.aboras@alexu.edu.eg
Amr Yousef,
✉ a.yousef@ubt.edu.sa
Mukesh Pushkarna,
✉ mukesh.pushkarna@gla.ac.in

RECEIVED 14 December 2023

ACCEPTED 11 January 2024

PUBLISHED 01 February 2024

CITATION

Pushkarna M, Govardhan Rao KV, Goud BS,
Kumar MK, Reddy CR, Kotb H, AboRas KM,
Alharthi YZ and Yousef A (2024), A new-fangled
connection of UPQC tailored power device
from wind farm to weak-grid.
Front. Energy Res. 12:1355867.
doi: 10.3389/fenrg.2024.1355867

COPYRIGHT

© 2024 Pushkarna, Govardhan Rao, Goud,
Kumar, Reddy, Kotb, AboRas, Alharthi and
Yousef. This is an open-access article
distributed under the terms of the [Creative
Commons Attribution License \(CC BY\)](#). The use,
distribution or reproduction in other forums is
permitted, provided the original author(s) and
the copyright owner(s) are credited and that the
original publication in this journal is cited, in
accordance with accepted academic practice.
No use, distribution or reproduction is
permitted which does not comply with these
terms.

A new-fangled connection of UPQC tailored power device from wind farm to weak-grid

Mukesh Pushkarna^{1*}, Kambhampati Venkata Govardhan Rao²,
B. Srikanth Goud³, M. Kiran Kumar⁴, Ch. Rami Reddy^{5,6},
Hossam Kotb⁷, Kareem M. AboRas^{7*}, Yahya Z. Alharthi⁸ and
Amr Yousef^{9,10*}

¹Department of Electrical Engineering, GLA University Mathura, Mathura, India, ²Department of Electrical and Electronics Engineering, St. Martin's Engineering College, Secunderabad, India, ³Department of Electrical and Electronics Engineering, Anurag University, Hyderabad, India, ⁴Department of Electrical and Electronics Engineering, Koneru Lakshmaiah Education Foundation, Guntur, India, ⁵Department of Electrical and Electronics Engineering, Joginpally B R Engineering College, Hyderabad, India, ⁶Applied Science Research Center, Applied Science Private University, Amman, Jordan, ⁷Department of Electrical Power and Machines, Faculty of Engineering, Alexandria University, Alexandria, Egypt, ⁸Department of Electrical Engineering, College of Engineering, University of Hafr Albatin, Hafr, Saudi Arabia, ⁹Electrical Engineering Department, University of Business and Technology, Jeddah, Saudi Arabia, ¹⁰Engineering Mathematics and Physics Department, Faculty of Engineering, Alexandria University, Alexandria, Egypt

A significant portion of wind power conversion systems worldwide comprise wind farms (WFs) that use Squirrel Cage Induction Generator (SCIG) and are directly linked to the power grid. In facilities that generate electrical energy at a moderate level, WFs are connected by means of distribution systems that use medium voltage (MV). It is not uncommon for such a system to produce a scenario in which the amount of electricity generated corresponds to the grid's transit volume. When a wind farm's wind power generation system is connected to a weak grid, the lack of potential control of the Point of Common Coupling (PCC) is a primary issue. This strategy is called a "Wind Farm with Weak Grid Connection." Therefore, the amalgamation of weak grids, fluctuating electricity from wind, and variations in load on the system cause disruptions in the PCC voltage, further degrading the Power Quality (PQ) and the WF stability. Either the control method at the production level or the compensating strategies at the PCC level can improve this situation. If wind farms are built on SCIG and are directly linked to the grid, it is essential to utilise the last substitute. The technology known as Custom Power Devices (CUPS), proved extremely helpful for this type of application. This study presents a compensation technique based on a specific CUPS device, known as the Unified Power Quality Compensator (UPQC), as a possible solution. The potential terminals of WF needed to be regulated, and the voltage fluctuations on the grid side required to be reduced, so a custom-made control strategy for the UPQC device was designed internally. The control of power, such as active and reactive in the UPQC's series and shunt converters, as well as the transmission of power via the UPQC DC-Link between converters, are the foundation of the internal control strategy that has been developed. Compared to other bespoke tactics that use reactive power, this strategy increases the UPQC's capability to provide compensation. The suggested study calculates THD using a FUZZY controller. The results are compared to PI controller results. Simulation findings show how the suggested compensating strategy can minimise

THD values and improve wind farm power and stability. The simulations suggest that the proposed compensating strategy enhances WF power and stability.

KEYWORDS

wind energy, UPQC, SCIG, voltage fluctuation, feeble grid, fuzzy

1 Introduction

The location of wind-generated electricity generating depends on wind energy. High-voltage (HV) transmission lines are usually far from these facilities (Xie and Sun, 2022). If the facility has medium power, medium voltage (MV) distribution wires will link the WF. The most distinguishing characteristic of these connections is an improved voltage control sensitivity to load variations (Huang et al., 2021). Therefore, the capability of the scheme to normalize potential at the PCC, which is the point at which the electrical system and the WF are coupled, is an essential factor in the proper operation of the WF. In addition, it is common knowledge that wind farms produce variable amounts of electric power due to the unpredictable nature of wind resources. These variations harm the consistency and quality of the electricity provided by the electric power systems (Song et al., 2023).

Additionally, SCIG-used wind turbines have been in use since the beginning of energy extraction from wind resources. The supply mains or capacitor banks supply the required reactive power with SCIG (Yang et al., 2024). There are fluctuations in the rotor speed. For example, the power grid's injected (demanded) WF active (reactive) power will fluctuate due to wind disturbances. This will produce variations in the WF terminal potential and the system's impedance. Electrical power turbulences will eventually find their way into the power system (Zhang et al., 2023), which may result in a spectacle known as a "flicker," which is characterised by oscillations in the level of illumination caused by voltage variations. Additionally, the regular operation of the WF is hampered by these disturbances. The effect is significantly more significant when "weak grids" (WG) are specifically considered.

Several potential methods have been proposed in demand to reduce the possible electric variations that can result in a "flicker" at the WF terminals. Updating the electrical grid by raising the power level at short circuits at the PCC is the most popular solution. This decreases system sensitivity to power fluctuations and voltage control issues (Liu et al., 2023).

Electronic equipment for electric power systems has become widespread due to high-power electronics technology. This device reacts faster than line frequency. FACTS and devices give these active compensators tremendous flexibility for controlling power flow in gearbox systems employing Custom Power System (CUPS) devices (Liu et al., 2023). This type of active compensator increased wind energy assimilation in weak systems, as researched (Miaofen et al., 2023).

We propose and test a UPQC-based compensation approach for a SCIG-based WF connected to a weak distribution power grid. This system is based on a study (Li et al., 2022a). The potential at the WF terminal can be controlled and the PCC experiences fewer voltage swings due to the management of the UPQC. These fluctuations are

caused by changes in the system load and the pulsating power provided by the WF, respectively. Inoculating the voltage "in phase" with the PCC potential, the series converter with UPQC controls the electrical potential at the WF terminal (Miaofen et al., 2023). This is achieved through voltage injection. Similarly, the parallel converter is utilised to screen the power created by the WF to prevent voltage swings. This function requires the ability to actively and reactively handle electricity. The standard DC link takes active power distribution among various converters (Chen et al., 2022). Simulations were carried out to demonstrate how successful the proposed compensatory strategy not only for UPQC and also verified with fuzzy logic controller.

1.1 Motivation

The literature survey, Table.1, shows that research has been carried out in the area of wind farms (WF) that use SCIG and are directly linked to the power grid. In facilities that generate electrical energy at a moderated level. Only a little research has revealed that wind farms are built on SCIG and are directly linked to the grid. It is essential to utilize for substitute. In this article, the technology known as CUPS, or custom power devices, proved extremely helpful for this type of application.

1.2 Literature review

A compensation technique that is based on a specific CUPS device known as the UPQC is presented in this study as a possible solution. The same is also implemented with a fuzzy logic controller and PI controller.

1.3 Contribution and organization of the paper

The main contribution of this paper is:

- The main technical characteristics of the weak grid are investigated in that WF is connected using distribution systems that use medium voltage (MV).
- The general case study of an electrical system with small WF with the parameters of 36 wind turbines for generating 21.6 MW electrical power.
- A dynamic layout of UPQC with complete switching converter involvement is developed.
- The complete controlling scheme of UPQC with Series and Shunt compensator is simulated.
- A new fuzzy logic controller is introduced into the system. These are tested with MATLAB Simulink to get a stable

TABLE 1 Literature analysis.

S. No.	Observation	Year	References
1	In this article equivalent modeling of doubly fed induction generator (DFIG)-based wind farms, the link between clustering indexes and sub-synchronous oscillation (SSO) modes and the difference in contribution to clustering results are rarely considered. This work presents a weighted fuzzy C-means (WFCM) clustering approach based on index dimension reduction. Furthermore, without considering the controller parameter coupling effects, a multiparameter coupling optimization design technique incorporating the response surface method and the orthogonal experiment method (OEM) is offered for the grid-connected system SSO study	2023	Song et al. (2022a)
2	This article explores the scope of this investigation, the mathematical model of a wind turbine is reduced in complexity by the utilization of a comparable transfer function. This paper also considers the corresponding line loss model of collector lines, classifies and builds up simplified wind turbines, and computes the corresponding amount of converged wind turbines using the improved capacity weighting method to create grid-connected reduced modelling of large-scale wind farms	2023	Song et al. (2022b)
3	This article explores how the stability of the power system in dual-fed induction wind turbines could be compromised by weak frequency modulation and input “source” disturbances. The computational model of the energy storage system integrated into the doubly fed wind power generation system compares the rotor kinetic energy and supercapacitor energy storage to supply inertia reaction power and energy. This is being done to fulfil the requirements of the system. After that, an evaluation of the multi-energy coordinated inertia response is carried out	2023	Zhu et al. (2022)
4	This article suggests a Quasi Z-Source Indirect Matrix Converter (QZSIMC) for Permanent Magnet Generator (PMG)-based Direct Drive Wind Energy Conversion Systems (DDWECS) to improve voltage transfer ratio and output voltage management under different loading situations. A three-phase Indirect Matrix Converter connects three Quasi Z-Source (QZS) networks to PMG and load in the QZSIMC. Two PWM control approaches, Carrier Based and Modified Space Vector, are proposed to analyze QZSIMC performance	2023	Lu et al. (2022)
5	This article proposes a football league algorithm-based hybrid controller trained by an artificial neural network controller (S-ANN) is presented for the shunt active power filter. This study offers a fuzzy logic controller for the UPQC’s series active power filter, which is connected to the solar photovoltaic and battery storage systems. A self-tuning filter (STF) and unit vector generation method (UVGM) synchronize phases to improve UPQC performance during unbalanced/distorted supply voltage conditions, eliminating the need for phase-locked loops, low-pass filters, and high-pass filters. The STF separates harmonic and fundamental components and generates series and shunt filter synchronization phases	2022	Sun et al. (2023)
6	This article deals with the virtual synchronous control (V_{sync}) technology. Wind turbines (WTs) may improve the damping coefficient, wind power permeability, and equivalent inertia by imitating the behavior of synchronous generators. Due to the challenging DFIG-grid coupling effect and the unusual partial-scale converter construction of the doubly fed induction generator (DFIG), grid-connected V_{sync} -based DFIG WTs have yet to receive much attention. Furthermore, unsteady V_{sync} modes may interact with the wind power system under unfavorable grid circumstances, influencing the dynamic characteristics of the DFIG and the system’s stability	2021	Yang et al. (2023)
7	This article explores the dynamic behavior of a grid-connected wind farm is described. The wind farm employs induction generators from squirrel cages, but the grid uses steam turbines. An energy capacitor device maintains the stability of the wind farm when the wind speed varies. The grid was linked to various load sizes to test the energy capacitor system controllers. Considering the participation of the grid load, the variations in the time constant of the integrated DC-DC chopper of the energy capacitor system were investigated	2021	Shirkhani et al. (2023)
8	This article explores the regional grid and DFIG-based wind farms can all transfer wind-thermal-bundled electricity employing a voltage source converter-based HVDC (VSC-HVDC). Together, the sending-end converter (SEC) of VSC-HVDC with PQ-control is susceptible to a new medium-frequency electrical oscillation since the local grid is often weak. This oscillation is caused by the interplay of the DFIG, local grid, and SEC; however, its exact mechanism is unclear. This paper derives an explicit analytic expression for the VSC-HVDC sending-end converter (SEC) sequence impedance model with the PQ-control outer loop and PLL. It then uses an intuitive analysis of the system impedance frequency characteristics to investigate the oscillation process	2021	Wang et al. (2023)
9	This article deals the frequent oscillations that the weakly grid-tied PMSG wind farms cause could pose a significant threat to the safety of the power system. The impedance-based technique is frequently used since it effectively improves the system; however, this method does not consider the PMSG’s function as a black box and merely reflects the quality of the system’s output on the outside. To enhance the research that has been done previously, this work proposes a unique impedance-based analytical method that can be used to examine weak-grid-tied PMSG wind farms from the perspective of control interaction	2021	Wang et al. (2022a)
10	This article explores the Sub-synchronous resonance (SSR). It is probable because of the impedance interactions between the wind farm, the weak grid, and the line-commutated converter-based high-voltage direct-current (LCC HVDC) at the sending end. The mechanism and characteristics of this SSR are analyzed using the impedance technique. SSR happens when the electricity generated by wind farms grows or the power used for LCC HVDC transmission drops. The studied technology quickly generates SSR as the transmitting end’s grid stiffness decreases	2021	Lin et al. (2023)
11	This article provides a steady-state analytic approach to assess the viability of WPP installation in site-specific locations based on grid connection parameters that transmission system operators often supply, such as reactance over resistance (X_{oR}) and short circuit ratio (SCR). The maximum active power transfer to the grid, the reactive power adjustment required for a stable and trustworthy grid connection under steady-state conditions, and weak grid situations are all determined by this feasibility study	2020	Wang et al. (2022b)

(Continued on following page)

TABLE 1 (Continued) Literature analysis.

S. No.	Observation	Year	References
12	This article deals about suppresses SSR using a synchronous compensator and a battery energy storage system (STATCOM/BESS) linked to the grid. A rising grid stiffness control method is presented, analogous to a virtual synchronous generator (VSG) for STATCOM/BESS with low active and high reactive power	2020	Li et al. (2022b)
13	In this study, an analytical investigation is performed to investigate how the weak grid connection influences the torsional sub-synchronous oscillations (SSOs) created by a grid-connected DFIG in a power system. These oscillations are caused by rotational inertia. The phase-locked loop (PLL) or DC voltage regulation is the primary focus of the investigation as it relates to the grid-connected DFIG operating in the SSO mode. A theoretical investigation is carried out to demonstrate that a poor grid connection intensifies the modal resonance effect between DFIGs and synchronous generators' torsional dynamics. When the grid connection is weak, the amplifying impact of the weak grid connection manifests as a decrease in the damping of the SSO mode of DFIG and an increase in the associated residue. Because of this, the DFIG has a more significant potential to create torsion SSOs under a poor grid connection, which might result in the system's instability in the worst possible scenario	2020	Duan et al. (2023)
14	This article of work aims to investigate the instability of the DFIG system while it is experiencing a weak grid failure by developing a micro-signal state-space model. Modal analysis reveals that the phase-locked loop (PLL), the rotor current control loop, and the terminal voltage are the factors that have the most significant influence on the dominating unstable poles that occur during the fault	2020	Xiao et al. (2023)
15	This study analyses how the control settings and active power outputs of grid-connected full-converter wind farms with low power affect sub-synchronous oscillation. Using Eigenvalue and participation factor analysis, we discovered the system's primary oscillation modes. Using the Eigenvalue technique, an investigation of the impact of control settings and active power output on the damping of sub-synchronous oscillations is carried out	2020	Hao et al. (2020)
16	A generic model and comparative study of grid-connected wind farms employing DFIGs in weak grids is presented in this paper. DFIG in a weak grid is benchmarked using a complete model. The model includes a generator, rotor side, converter, phase-locked loop, and mechanical parts. Two simplified models of grid-connected DFIG-based wind farms in a weak grid are compared to the full model using linear system analysis to study sub-synchronous oscillation (SSO) and its causes	2020	Yan et al. (2020)
17	In this study a wind energy generating system (WEGS) that can reach peak output in variable wind speeds without frequency variations was studied. The machine-side voltage source converter (MSVSC) and utility grid-side voltage source converter (UGVSC) are successive VSCs positioned across the DC-link capacitor. These VSCs adapt generator speed to intermittent wind speeds. This study's hybrid generalized integrator control can improve power quality, eliminate sub-harmonic oscillations, and switch UGVSC. A fuzzy logic controller (FLC) controls a wind turbine's salient pole synchronous generator (SG) speed. The FLC monitors reference speed despite restricted bandwidth and high overshoot transients. MSVSC switching uses field-oriented control	2020	Chishti et al. (2020)
18	This study examined the SSO mechanism of D-PMSG-based wind farms using impedance-based stability analysis. An impedance model of grid-connected D-PMSG is created utilizing harmonic linearization theory in the first part of this research effort. Next, sub/sup synchronous current coupling is statistically studied for the first time. We explain how grid impedance and wind farm operational factors affect stability using the impedance model and relative stability criteria	2019	Yuan et al. (2019)
19	In this study, The work evaluated the SSO mechanism of D-PMSG-based wind farms using impedance-based stability analysis, a standard method. First, a grid-connected D-PMSG impedance model based on harmonic linearization theory is built, and the sub/sup synchronous current coupling is assessed. The relative stability criterion and impedance model characterize grid impedance and wind farm operational factors' effects on stability	2019	Sang et al. (2019)
20	Integrating large-scale wind power is a challenge for today's electricity networks. Therefore, simpler, more accurate wind farm (WF) models are required. Aggregation is used in WF modeling to save processing time and model complexity. The fully aggregated model (FAM) and multimachine model, which split the WF into many aggregated models for different sections, are used in the literature. This article compares the two aggregation strategies using a small-signal model	2018	Morgan et al. (2018)

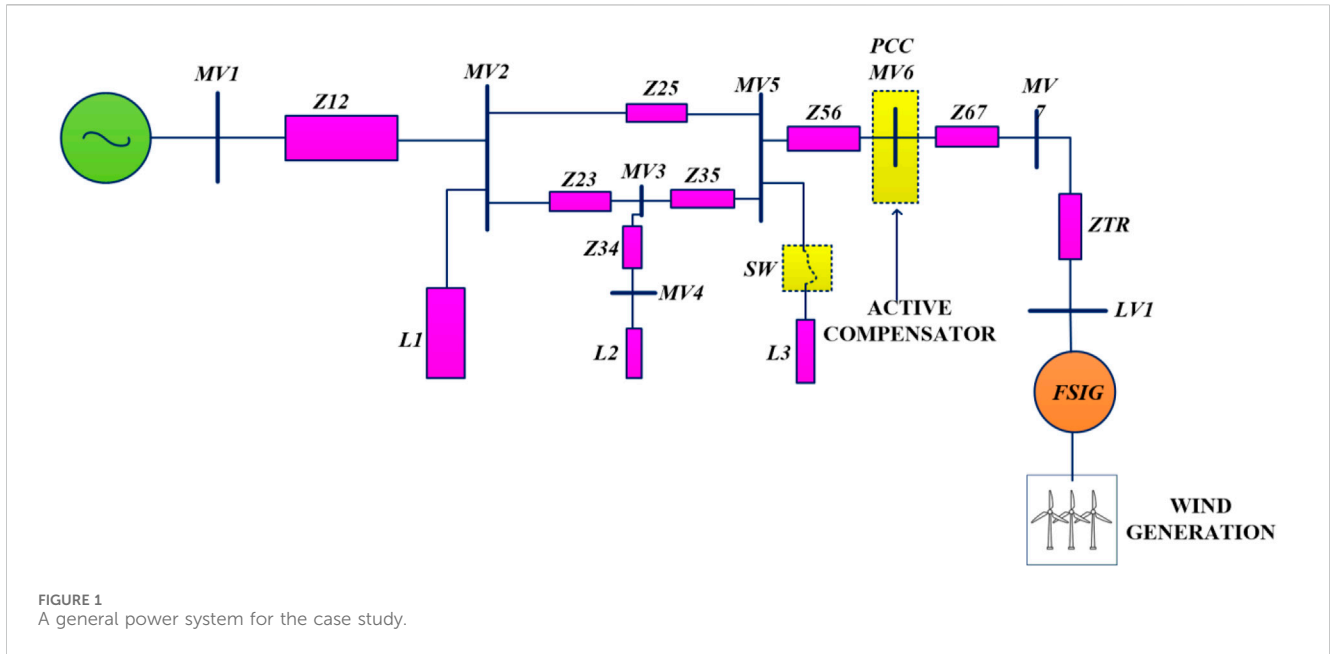
operation to improve voltage WF in the weak grid, and THD results are also presented.

This paper is organized with an abstract on keywords. In the first section, the introduction is explained in terms of wind forms with different UPQC and fuzzy techniques, followed by the literature survey and the paper's contribution. The second section discusses the general case study in the electrical system. In the third section, the turbine rotor and disturbance model are discussed. In the fourth section, the proposed layout of the dynamic compensator model of the induction generator is developed. The fifth and sixth section consists of control scheme for UPQC and fuzzy implementation techniques. The seventh section deal with results and discussion The eighth and ninth sections deal with discussion for paper outcome, followed by an explanation of the conclusion.

2 General case study explanation of electrical system

The electrical system being looked at in this research can be seen in [Figure 1](#). The WF comprises 36 wind turbines utilising squirrel cage induction generators, producing 21.6 MW of electrical power. Each turbine is coupled to an electrical grid of a 630 kVA 0.69/33 kV transformer and features attached fixed reactive compensation capacitor banks with a rating of 175kVAr. Based on reference ([Liu et al., 2018](#)), this system depicts a real-life scenario.

The indication of the "connection weakness" based on the power ratio during a quick circuit to the power-valued WF. Consequently, while taking into consideration the fact that the short circuit power in MV6 is $S_{SC} > 120 \text{ MV A}$, so this ratio can be calculated with (1).



$$r = \frac{S_{SC}}{P_{WF}} \cong 5.5 \tag{1}$$

Any value of $r < 20$ is regarded as having a “weak grid” linkage (Nie et al., 2022).

3 Turbine rotor and associated disturbances model

The following expression determines the amount of electricity obtained from a WT:

$$P = \frac{1}{2} \cdot \rho \cdot \pi \cdot R^2 \cdot v^3 \cdot C_p \tag{2}$$

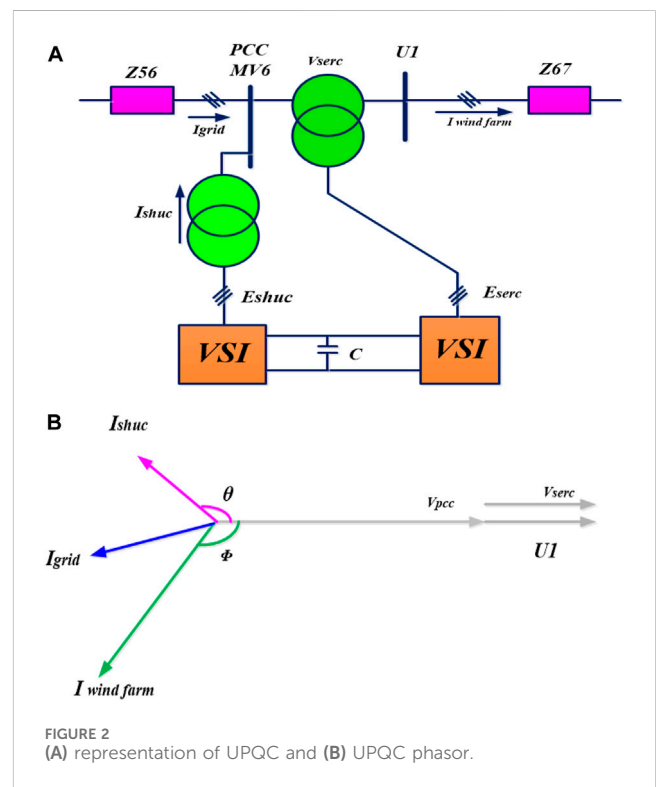
Where ρ is the air density, R is the radius of the swept area, v is wind speed, and C_p is the power coefficient.

For the considered turbines (600 kW), the values are $R = 31.2$ m, $\rho = 1.225$ kg/m³ and C_p calculation is taken from (Damchi and Eivazi, 2022).

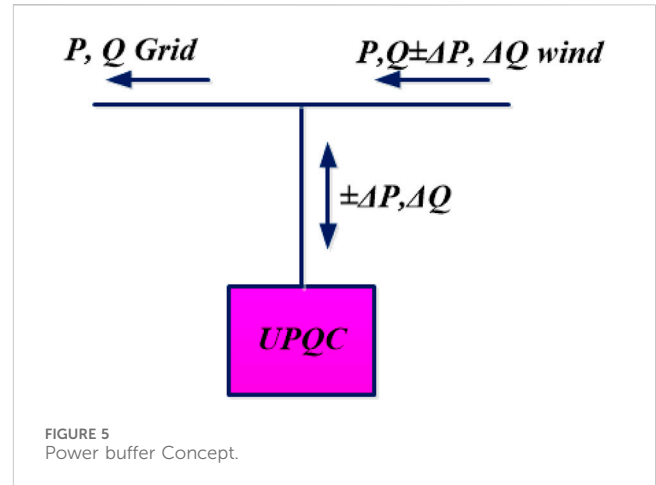
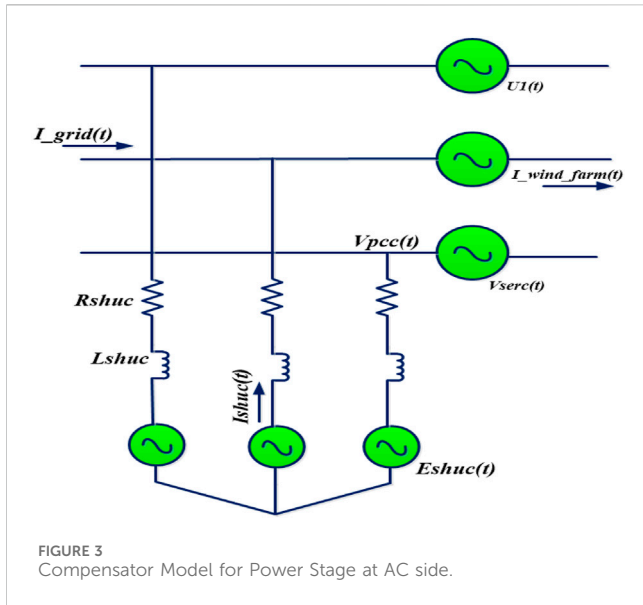
The power from the turbines is then combined to create a comprehensive model of the WF, showing that the entire WF is represented by a single corresponding turbine producing electrical potential from wind power, which is the same as the mean totality of the power provided by each turbine is expressed in (3):

$$P_T = \sum_{i=1,2,3,\dots,36} P_i \tag{3}$$

In addition, disruptions in the wind flow can cause the wind speed v in (2) to fluctuate about its usual value. The first is determined by an irregularity in the stream of air that is “seen” from the blades of the turbine because of “tower shadow” and/or edge coat of the atmosphere, and the second is caused by erratic changes that are referred to as “turbulence.” Both of these factors can



affect the energy produced using the wind turbine. Consider disruption to the airflow induced by the support structure (tower) as part of our analysis. When applied to the mid value of v , the disruption is viewed as a sinusoidal modulation. This modulation has a frequency of N_{rotor} for the three-bladed WT, and the breadth depends on the tower’s design. An amplitude modulation of 15% and an average 12 m/s wind speed is used (Rao et al., 2023).

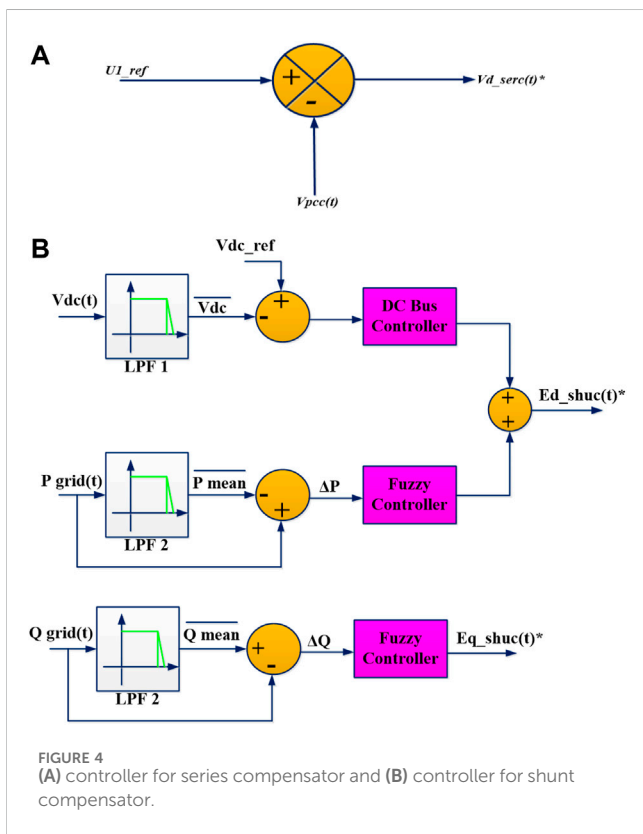


4 Typical layout of dynamic compensator model induction generator

The model used for the SCIG is the one that is included in the Matlab/Simulink, Sim Power Systems package (Venkata Govardhan Rao et al., 2022). Dynamic voltage fluctuations are accounted for by supplying the MV6 (PCC) bus bar with potential in series and active reactive power. This is accomplished with a unified type compensator, a UPQC (Ray et al., 2021). The general layout of this compensator can be seen in Figure 2A, while Figure 1 should be used as a reference for the bus bar and impedance numbering.

The process involves utilising VSI or CSI electrical converters to create three-phase voltages. As for its lower loss of DC link and quicker system response, the VSI converter is preferred over the CSI converter (Srikanth et al., 2023). The UPQC's shunt converter is accountable for injecting current at PCC, as explained in Figure 2B, while the series converter produces electric potential for PCC and UI. The vital theme of the compensator is that the series and shunt VSIs operate using the same DC bus. Thanks to this functionality, the two different types of converters can actively transfer power.

The converters are manufactured using ideal regulated voltage sources since the switching control of the converters is outside the purview of this work, and the higher-order harmonics produced by VSI converters are outside the bandwidth of importance in the simulation analysis. It is completed since the switching converter control is not involved in this task. Figure 3 displays the finalized model of the UPQC system's power side.



In most situations, the effect of the edge coat of the atmosphere is disregarded in favour of the results provided by the shadow effect produced by the tower (Yang et al., 2015). Note that the total of perturbations can occur if the entire turbines operate in the same sequence and in phase, which has the most significant impression on the electrical grid (worst case scenario) because the pulsation of power has the most significant peak in this situation. Therefore, the turbine combination method is acceptable.

$$T = \frac{2}{3} \begin{bmatrix} \sin(\Theta) & \sin\left(\Theta - \frac{2\pi}{3}\right) & \sin\left(\Theta + \frac{2\pi}{3}\right) \\ \cos(\Theta) & \cos\left(\Theta - \frac{2\pi}{3}\right) & \cos\left(\Theta + \frac{2\pi}{3}\right) \\ \frac{1}{2} & \frac{1}{2} & \frac{1}{2} \end{bmatrix} \quad (4)$$

$$\begin{bmatrix} f_d \\ f_q \\ f_0 \end{bmatrix} = T \cdot \begin{bmatrix} f_a \\ f_b \\ f_c \end{bmatrix} \quad (5)$$

Where $f_i = a, b, c$ represents either the phase voltage or current, and $f_i = d, q, 0$ represents that magnitude transformed to the $dq0$

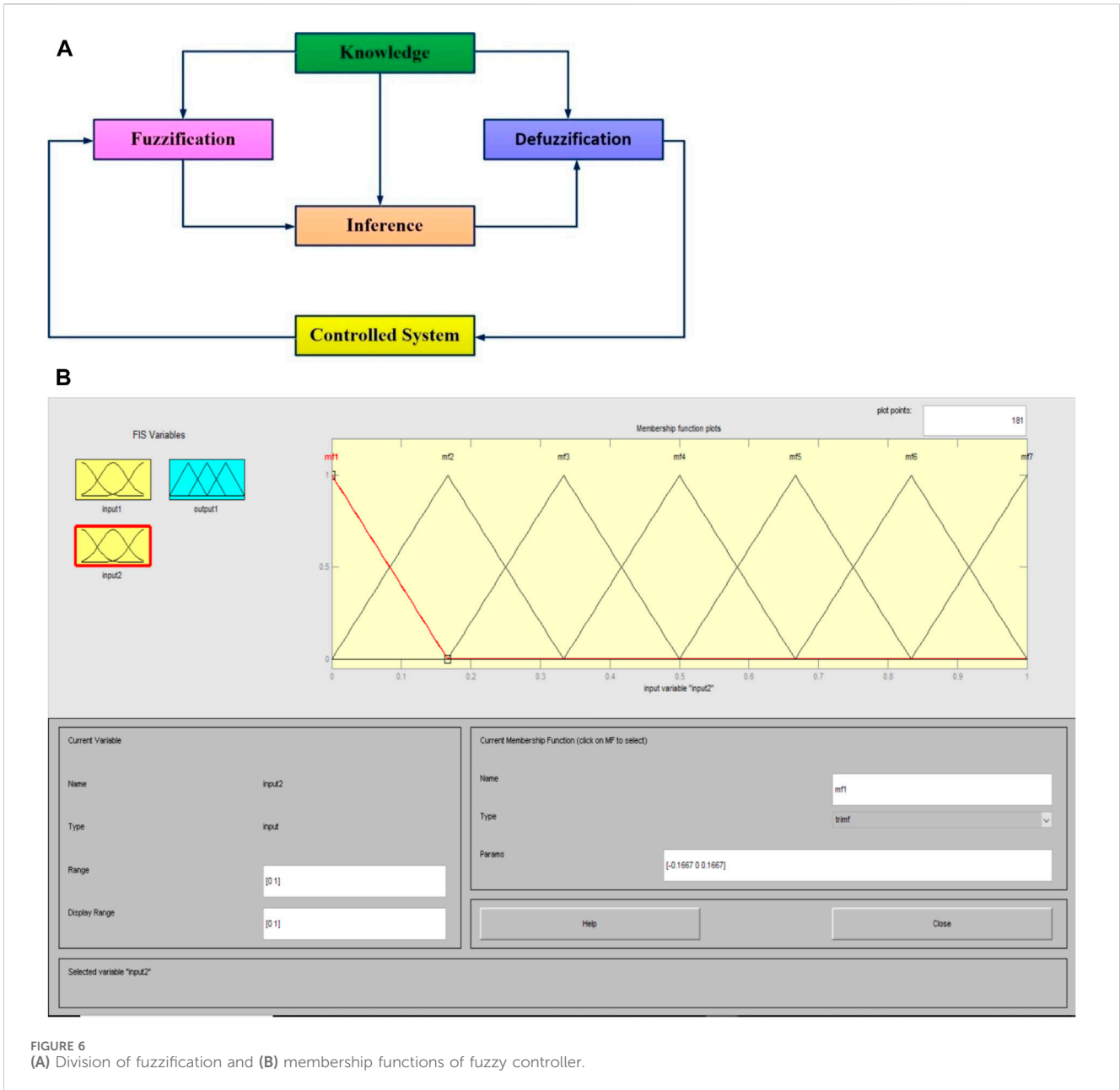


FIGURE 6 (A) Division of fuzzification and (B) membership functions of fuzzy controller.

TABLE 2 Fuzzy rules for this case.

E(K), ΔE	NB	NM	NS	ZE	PS	PM	PB
NB	NB	NB	NB	NB	NM	NS	ZE
NM	NB	NB	NB	NM	NS	ZE	PS
NS	NB	NB	NM	NS	ZE	PS	PM
ZE	NB	NM	NS	ZE	PS	PM	PB
PS	NM	NS	ZE	PS	PM	PB	PB
PM	NS	ZE	PS	PM	PB	PB	PB
PB	ZE	PS	PM	PB	PB	PB	PB

From Table PB: positive big, PM: positive medium, PS: positive small, ZE: zero, NS: negative small, NM: negative medium, NB: negative big.

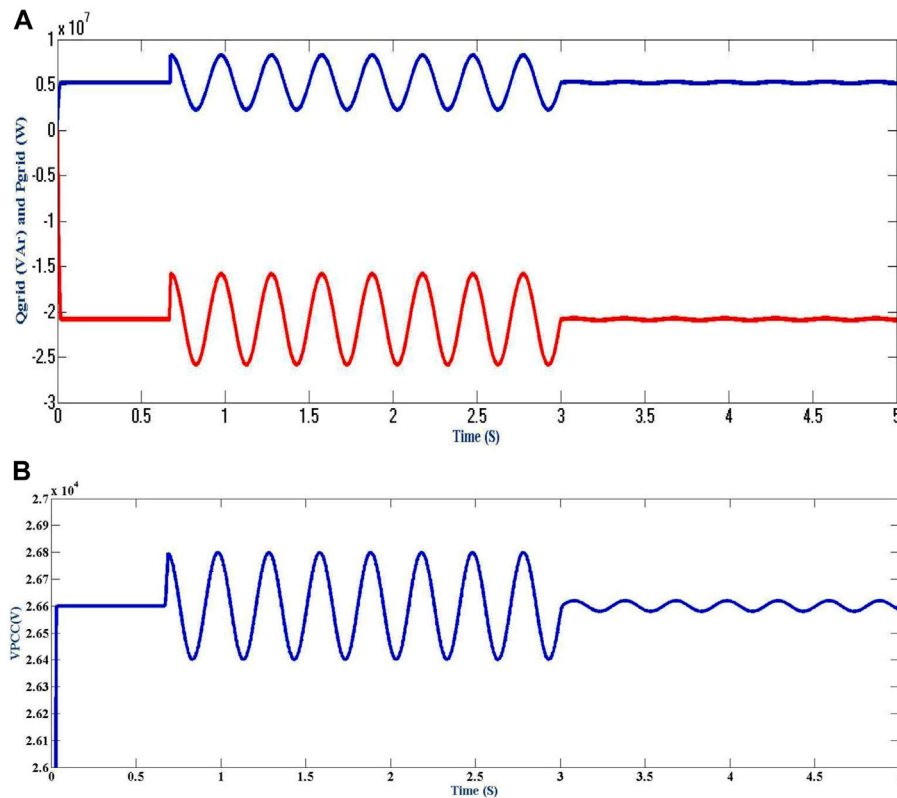


FIGURE 7 (A) Active and reactive power demand's power component at the power grid side and (B) Electric Potential at PCC.

space. The controlling of UPQC, with rotating frames using a park's transformation is mentioned in (4) & (5).

It enables the position of a reference frame of the rotating body in the positive direction of the PCC potential space vector. A PLL mechanism determines a reference angle synchronism with the PCC positive sequence fundamental voltage space vector. This makes it possible to get the desired outcome. This study has a PLL that is examined using the "instantaneous power theory".

Under balanced and equilibrium conditions, the synchronous reference frame's electric potential and current vectors do not change. This quality is advantageous for study and detached control.

5 Control scheme for UPQC

The WF terminal voltage is maintained at its nominal level by managing the UPQC serial converter (as in Figure 3), which makes up for variations in the PCC voltage. If this is done, the grid-generated voltage disturbances will not be able to reach the WF facilities. If voltage dips occur at the WF terminals due to this control action, it may have the unexpected impact of increasing the LVRT capacity.

Figure 4A explains the series converter controller block diagram. The PCC electric potential is subtracted from the reference electric potential to produce the injected electric potential, which is aligned in phase with the PCC electric potential. The voltage is injected as a result. On the other hand, the UPQC uses its shunt converter to mesh the pulsations of active and reactive power components, which WF causes.

As a result, there will not be any pulsations in the electricity that the WF compensator set injects into the grid. Pulsations cause voltage fluctuations that may propagate throughout the system. This action can be finished with the correct electrical current injection into the PCC. Additionally, this converter has been able to normalize the voltage on the DC bus.

The block architecture of the shunt converter controller is displayed in Figure 4B. The voltage instructions of E_{d_shuC} and E_{q_shuC} are produced in this way, depending on the variations ΔP and ΔQ , respectively. The deviations are computed by deducting the mean power from the instantaneous power measured in PCC. Filing by low pass filter calculates the expected values of the active and reactive power components. These filters' bandwidths are altered such that, by the IEC61000-4-15 standard, the fluctuation components for power are chosen as they lie in the flicker band and accept compensation.

Additionally, the control action for the DC-bus voltage loop is contained within E_{d_shuC} since its components operate at a frequency that is lower than that of the flicker-band.

In the rotating reference frame, the powers P_{shuC} and Q_{shuC} are computed as follows in (6):

$$\begin{aligned}
 P_{shuC}(t) &= \frac{3}{2} \cdot V_d^{PCC}(t) \cdot I_d^{shuC}(t) \\
 Q_{shuC}(t) &= -\frac{3}{2} \cdot V_d^{PCC}(t) \cdot I_q^{shuC}(t)
 \end{aligned}
 \tag{6}$$

The equations other than PCC voltage variation, can be expressed as follows in (7):

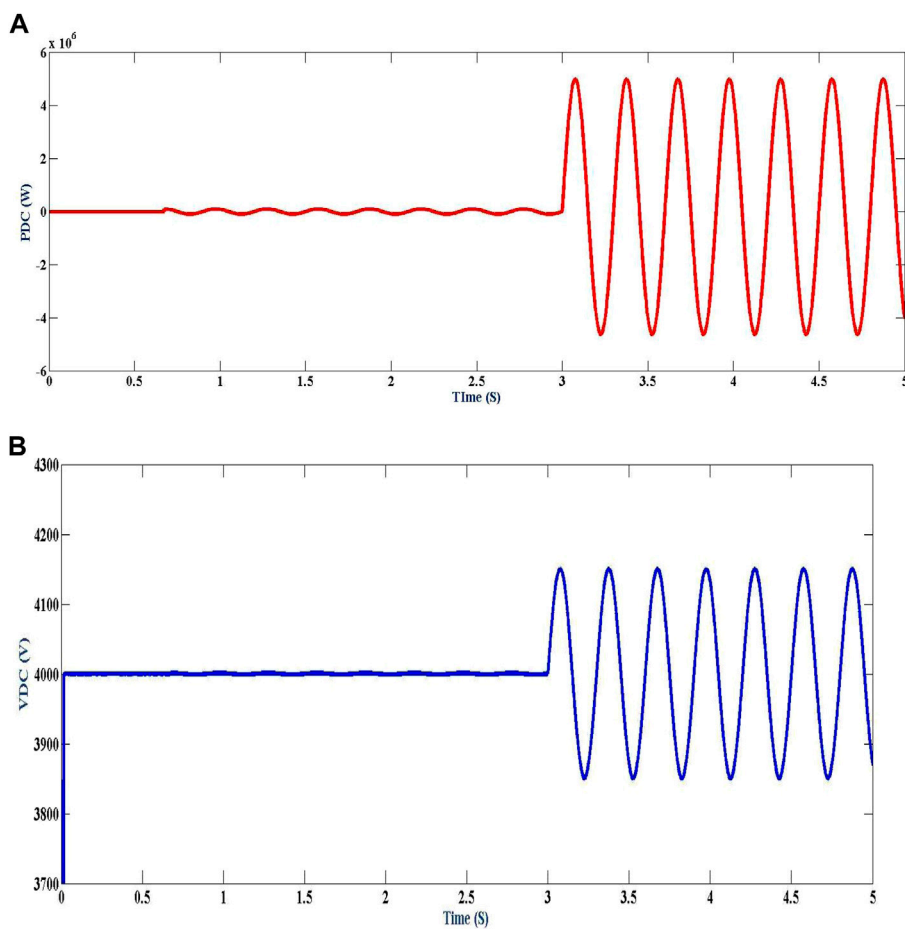


FIGURE 8 (A) Power in the capacitor of DC bus and (B) Voltage in the capacitor of DC bus.

$$\begin{aligned}
 P_{shuC}(t) &= k_p' \cdot I_{d-shuC}(t) \\
 Q_{shuC}(t) &= k_q' \cdot I_{q-shuC}(t)
 \end{aligned}
 \tag{7}$$

Given that the shunt converter is built around a VSI, we must produce sufficient voltage to attain the currents in (6). It is possible by the model of VSI, which is discussed in (Song et al., 2022a), which leads to a linear relationship between the power output and the controlled voltages. Following are the resultant equation in (8):

$$\begin{aligned}
 P_{shuC}(t) &= k_p'' \cdot E_{d-}^*(t)_{shuC} \\
 Q_{shuC}(t) &= k_q'' \cdot E_{d-}^*(t)_{shuC}
 \end{aligned}
 \tag{8}$$

Proportional controllers have examples of P and Q control loops, whereas the DC-bus loop is an example of a PI controller.

In a nutshell, UPQC is considered a “power buffer” in the suggested strategy, which helps to equalise the power inoculated into the power system grid. This style of operation is conceptually represented by a schematic, which may be found in Figure 5.

It is crucial to remember that the storage element installed on the bus containing UPQC must uphold its mean power at zero because the bus lacks an external DC supply. This is the situation to protect the system’s integrity. To do this, a well-designed DC voltage controller is essential.

The concept of power buffer may not be executed with a DVR; however, it is possible to do so with a DSTATCOM. A DVR device is more appropriate in this situation than DSTATCOM’s solution since voltage regulation during moderately significant disturbances cannot be effectively managed with just DSTATCOM’s reactive power.

6 Implementation of fuzzy logic controller (FLC)

The enormous potential of fuzzy set theory for effectively addressing the problem’s uncertainty is evident (Raju and Rao, 2015). It is an outstanding mathematical tool for handling ambiguity-related uncertainties. The concept of fuzzification and de-fuzzification is explained in Figure 6A, and the membership functions of fuzzy controller are depicted in Figure 6B.

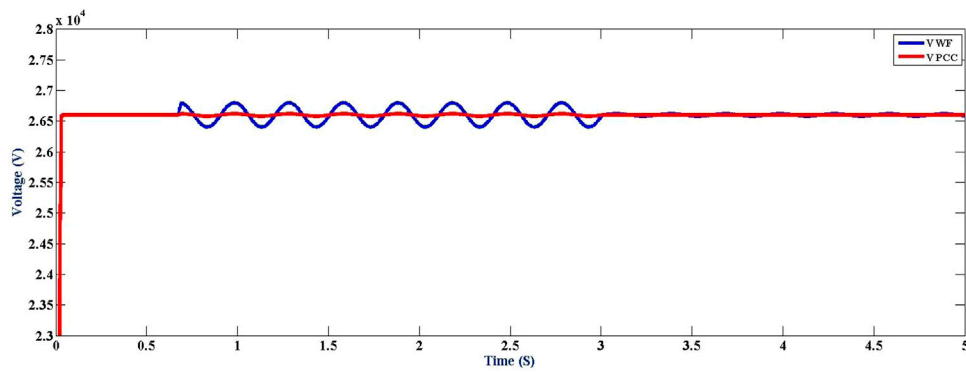


FIGURE 9 Electric Potentials of WF and PCC are shown in phase.

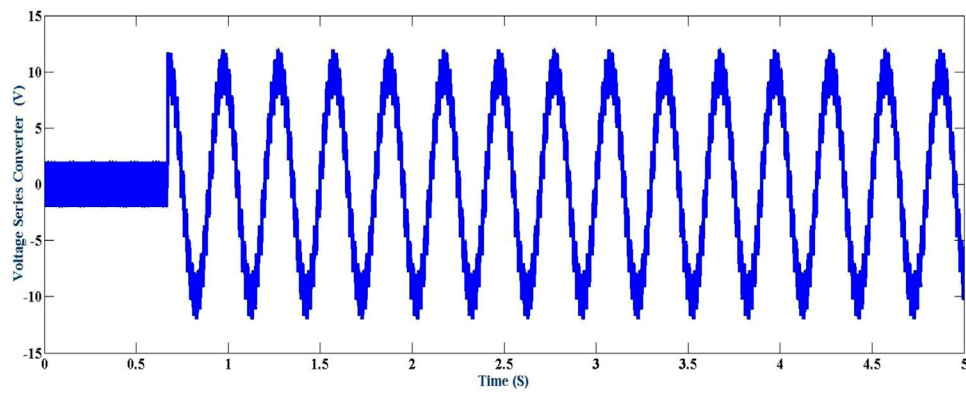


FIGURE 10 Series injected electric potential for the "a" phase.

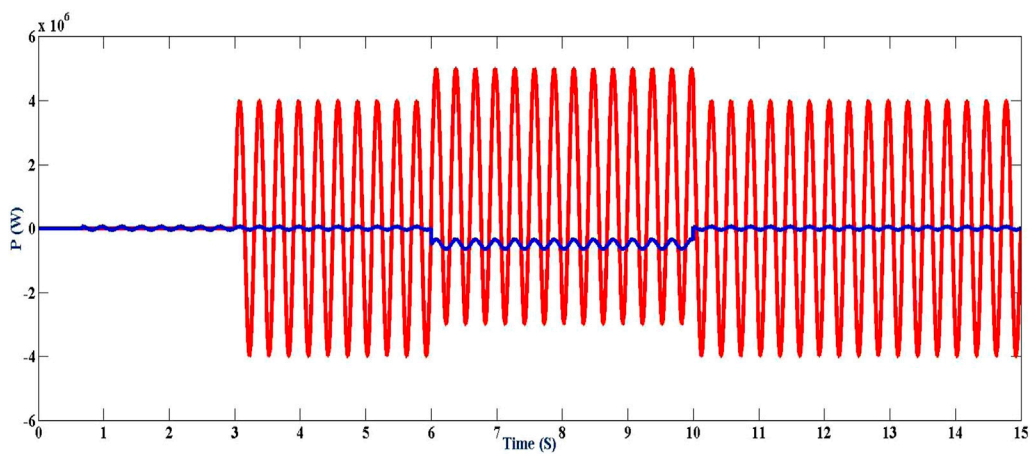


FIGURE 11 DC bus shunt and series active power.

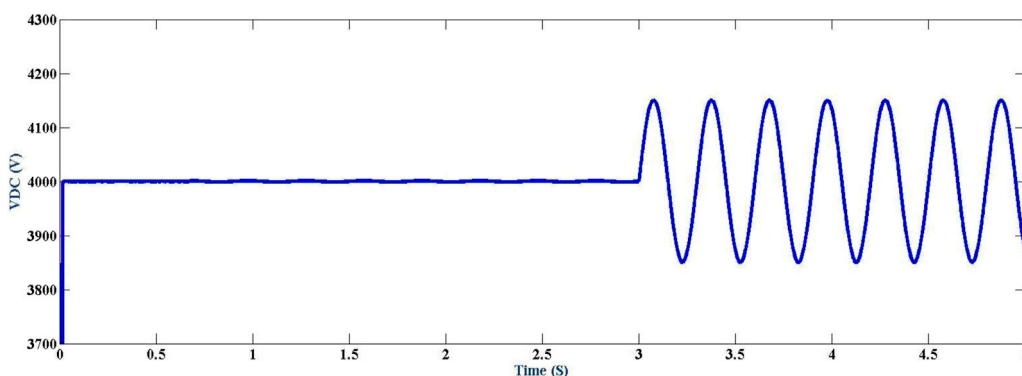


FIGURE 12 Bus potential at DC.

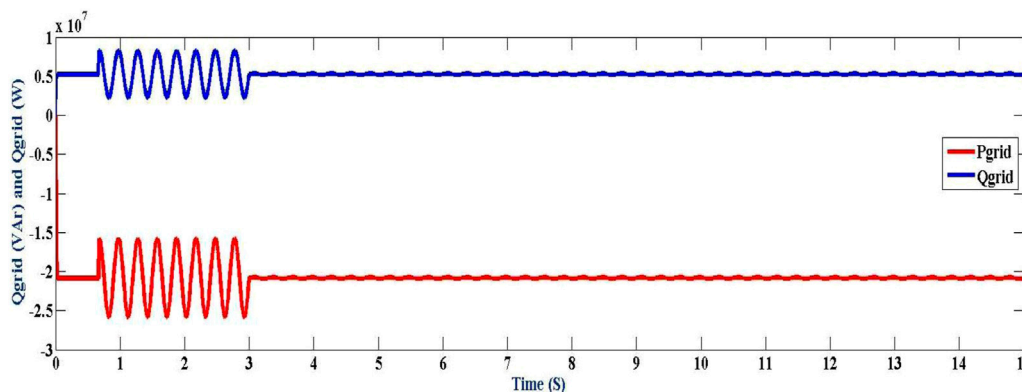


FIGURE 13 Power grid-side active and reactive power consumption.

6.1 Error calculation

The difference between the value as it is now and the reference value that the repeated controller created helps calculate the error signal ($errA$). Additionally, the R_{errA} represents the variance in error in the current sampling and its prior sampling. These current signals are measured and transformed to per unit (p.u.) values for each phase.

6.2 FLC

Three subsections make up the FLC section. The following is a summary of these subsections..

6.3 Fuzzification

The fuzzy linguistic variable, which has a crisply defined border, is created by fuzzifying the numerical input variable

measurements, and Table 2 reflects the fuzzy rules for using this fuzzification.

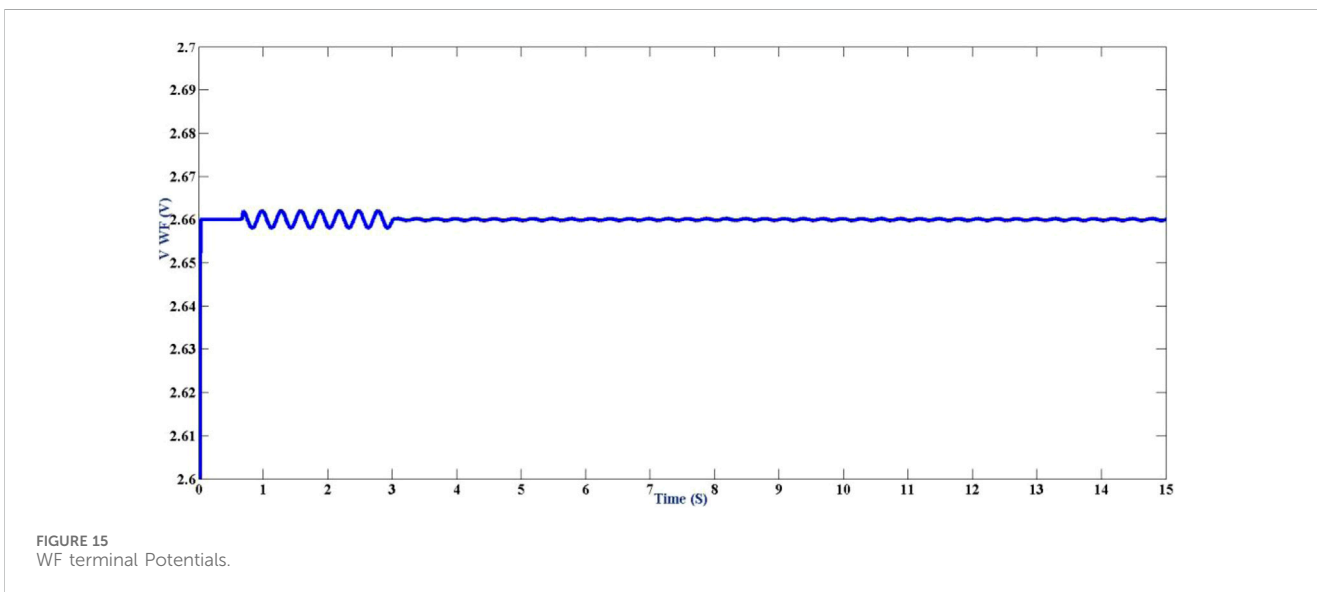
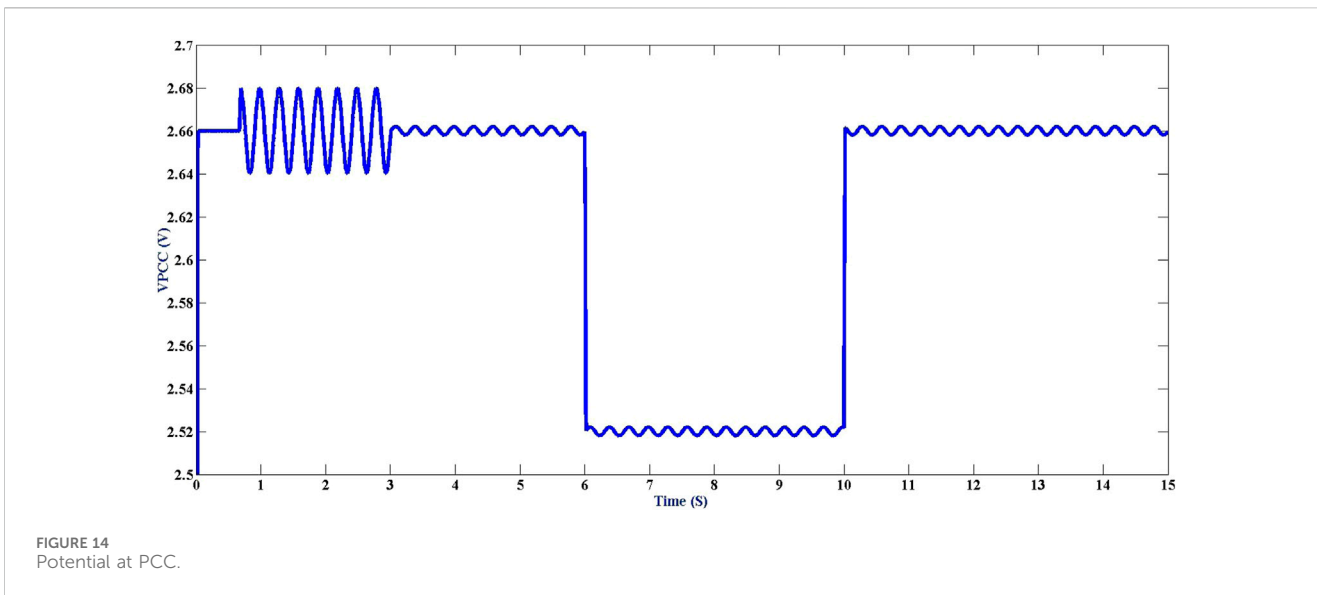
6.4 De-fuzzification

Previously represented as linguistic labels by a fuzzy set, the controller outputs are transformed into actual control (analogue) signals during de-fuzzification. For the fuzzy model’s de-fuzzification procedure, the “Sugeno’s Weighted Average” method, a particular application of the “Mamdani Model,” is employed.

Signal processing: The FLC process output creates the control signals. They are compared to the carrier signal to produce switching signals for converters.

7 Results and discussions

Matlab/Simulink software was used to create the prototypical view of the power system scheme depicted in Figure 1. The



controllers and the control strategy described in Section III are included in this model. Numerical simulations were carried out to determine and compensate for the voltage fluctuation brought on by variations in wind power and voltage regulation difficulties brought on by a sudden load hook-up.

7.1 Electrical potential fluctuation compensation

Figure 7 displays the simulation results for 0–5 s. The cyclical power pulse the tower shadow effect creates starts when time equals 0.5. As was already established, the tower shadow changes torque, affecting the WF’s active and reactive power components. The

frequency of power variation at the minimum wind speed is $f = 3.4 \text{ Hz}$, and the resulting magnitude of the electric potential variation at PCC is in (9):

$$\frac{\Delta U}{U_{rated}} = 1.50\% \tag{9}$$

For 0.5 to 3, the middle curve of Figure 7A shows this voltage fluctuation. The fluctuation’s value exceeds the IEC standard’s maximum allowable limit (Zhu et al., 2022). This shows that the WF has a detrimental effect on the System Power Quality even when everything operates smoothly.

P, Q controllers are turned on at time $t = 3.0''$, which causes the pulsations of active and reactive power to slow down. The PCC voltage fluctuation’s amplitude has decreased from its prior value of

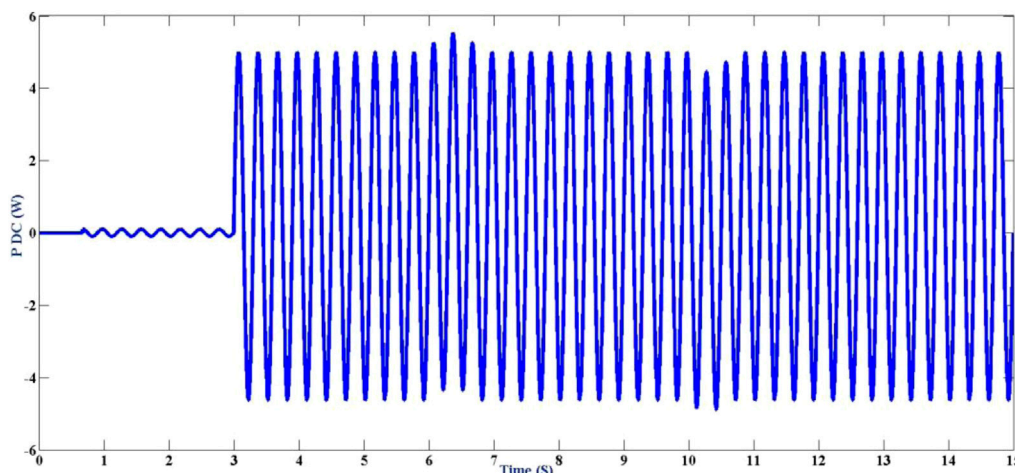


FIGURE 16 Power in the capacitor at the DC bus.

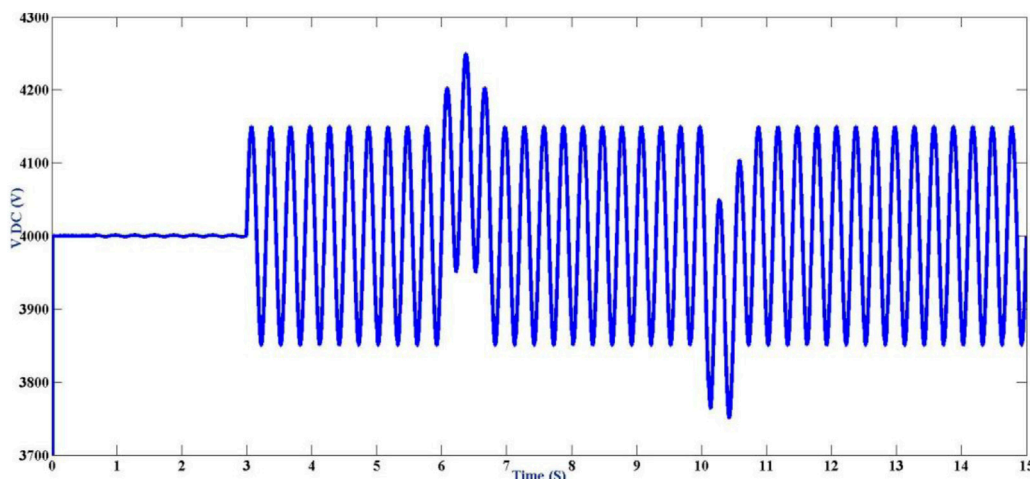


FIGURE 17 Capacitor potential in the DC bus.

1.6% (without correction), which was previously used, to this new amount.

$$\frac{\Delta U}{U_{rated}} = 0.18\% \tag{10}$$

Given that it is less than the set permitted maximum limit of 0.5% at 3.4Hz, this number complies with the requirements of the IEC standard.

Figure 7A illustrates the active and reactive power and voltage pulses on the DC side of the UPQC. As can be seen from Figure 7A, the series converter needs very little power to run. However, the shunt converter needs a high instantaneous power level from the

capacitor to compensate for changes in active power. The DC side power is unaffected by reactive power compensation. The behaviour of the WF terminal potential is depicted in Figure 7B. The series converter action keeps the WF terminal potential constant independent of the PCC voltage’s behaviour.

According to VSI’s operational features, the voltage level on the DC bus is capped at a specific level. Because the capacitor is in charge of managing the fluctuating active power, the value of the capacitor must be selected so that the DC electric potential “ripple” is in the specified margin.

For instance, a capacitor with a size of $C = 0.42\text{ F}$ has been considered. It is simple to quickly obtain this high value by utilizing capacitors based on modern technology, known as ultracapacitors.

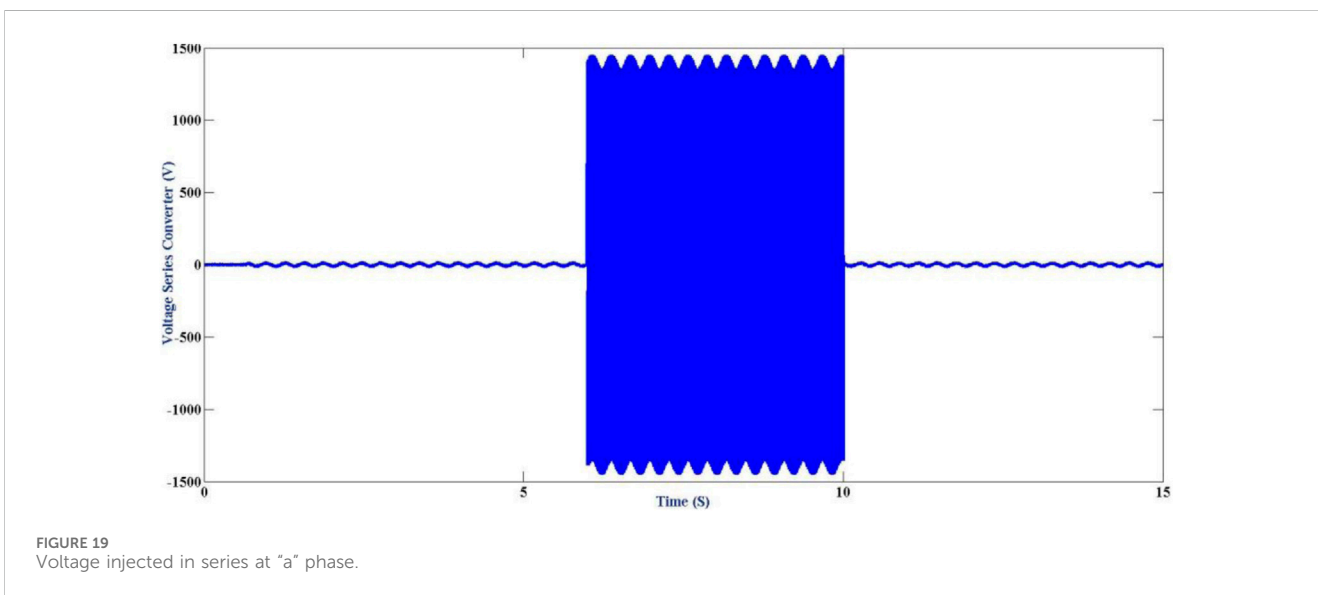
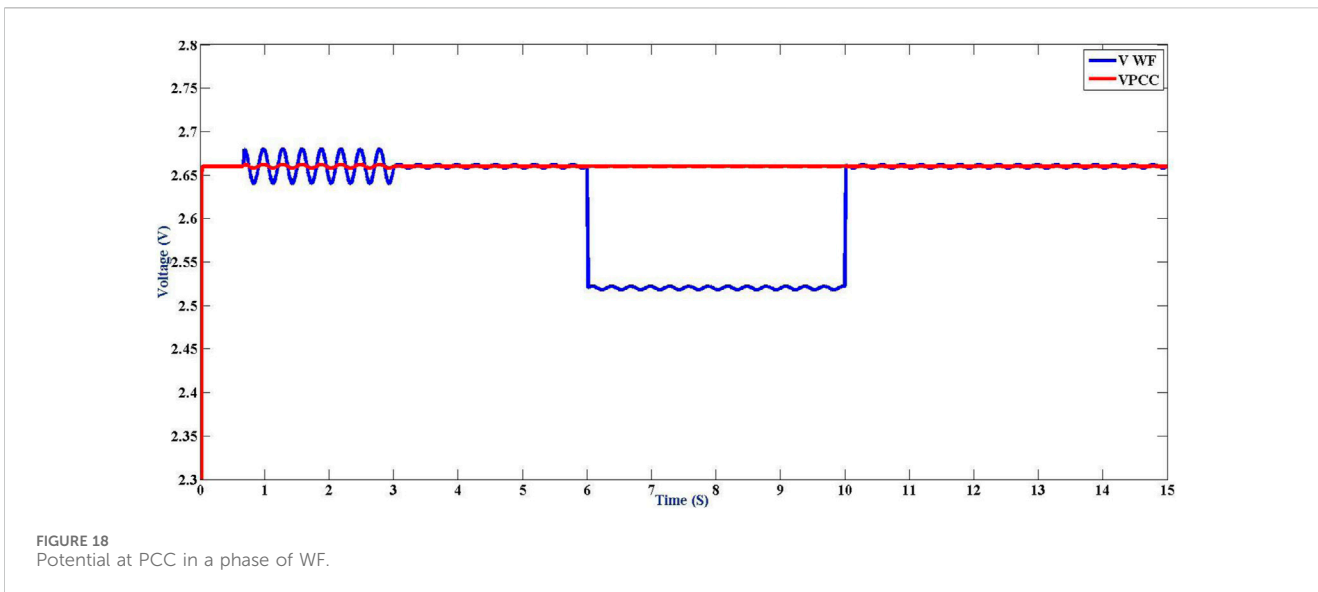


Figure 8A shows the power in the capacitor of the DC bus, and Figure 8B shows the voltage in the capacitor of the DC bus. It is crucial to remember that when the grid's measured current flows towards the park, it is optimistic.

7.2 Regulation of electric potential

The UPQC is used in this section to maintain the steady WF terminal potential while concurrently reducing PCC electric potential variations caused by abrupt engagement or disengagement of loads, power system malfunctions, and other difficulties. At the time $t = 6''$, the switch labelled SW to L3 is closed, which results in a sudden connection of the load in Figure 1. This load has a PL3 rating of 9.2 MW and a QL3

rating of 9.25 MW. After then, the load is disconnected at a time equal to 10 s.

Power in the capacitor terminal voltages and the series injected voltage are displayed in Figure 9 for the "a" phase. Because of the action of the series converter, the figure shows a dramatic shift in the voltage at the PCC terminals, while the voltage at the WF terminals remains practically unchanged. As a result, the active power stage for a series converter is the same as the power for a shunt converter but has the opposite sign. Figure 10 and Figure 11 also explain the DC-bus voltage and the control action of VDC, both of which are extremely obvious. VDC's mean value is maintained at the reference level. However, the ripple is not muted.

The midpoint power injected or engrossed by the series converter is inserted or absorbed by the converter in a shunt as a

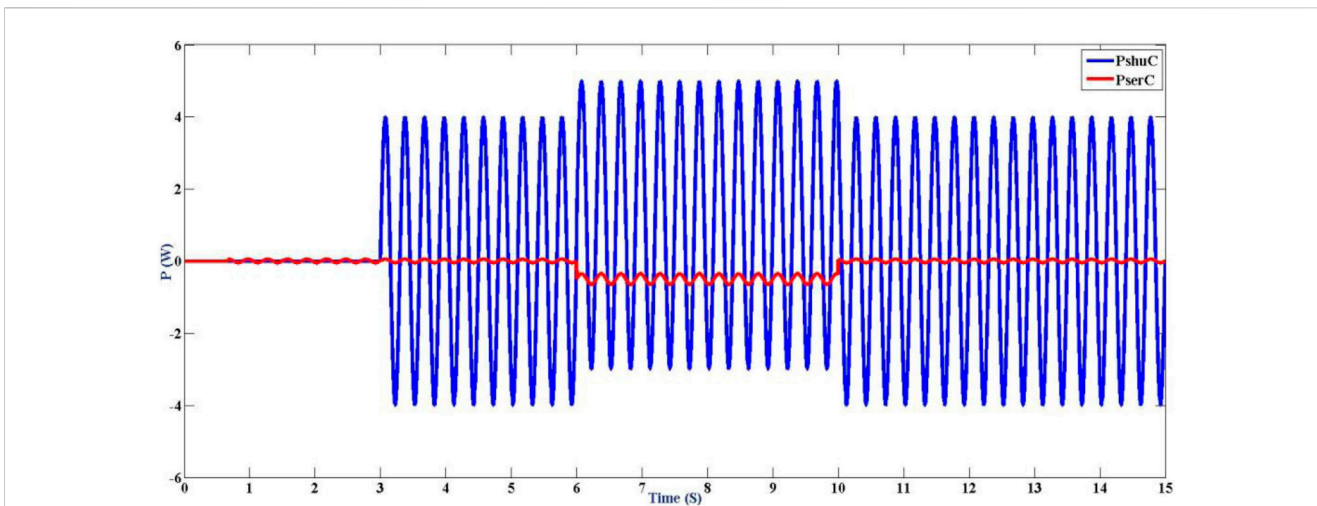


FIGURE 20 The DC bus's shunt power and series power.

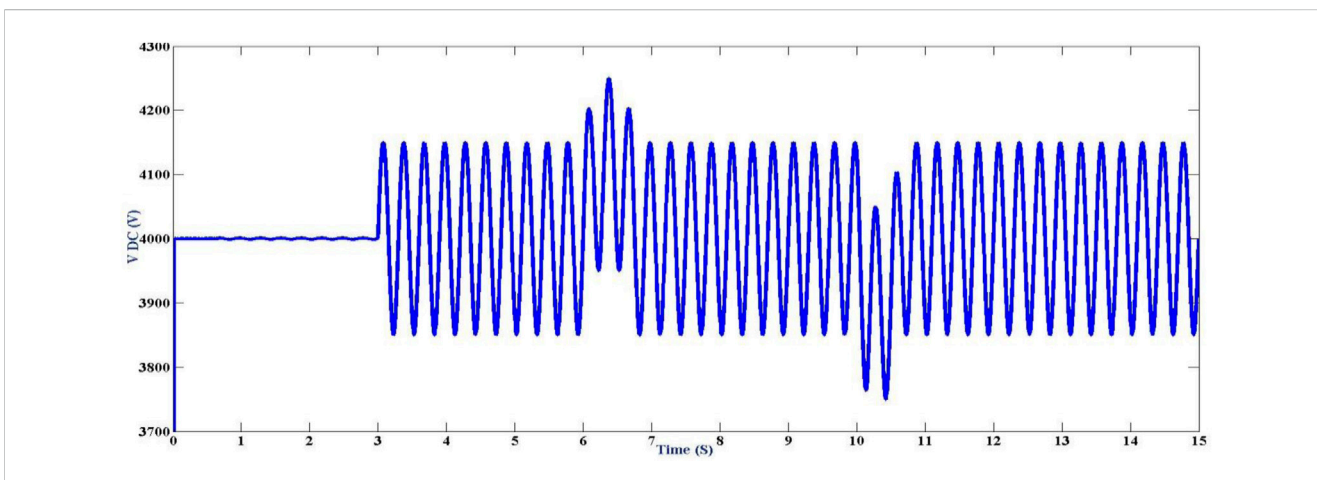


FIGURE 21 DC bus voltage.

result of the functioning of the loop for regulating DC voltage depicted in Figure 12.

7.3 By using a fuzzy controller

The analysis was repeated by using a fuzzy controller and the results can be shown from Figure 13 Figure 14 Figure 15 Figure 16 Figure 17 Figure 18 Figure 19 Figure 20 to Figure 21.

8 Discussion of paper outcome

The UPQC and fuzzy logic controller results clearly illustrate the power demand potential of the PCC series and shunt compensators' injected power. However, here, we proposed a fuzzy logic controller implementation to the same system; with this, we are maintaining all

the parameters are the same, but the THD value of the Fuzzy system with the PI controller is meagre, i.e., 2.81% in comparison to the UPQC system of 5.13%. Shown in Figure 22A,B, the outcomes of the simulations demonstrate that the proposed compensation technique is beneficial in improving the Quality of power and stability in WF.

9 Conclusion

The article presents a newfangled compensation stratagem built by a UPQC compensator to link SCIG wind farms to feeble power grids. The recommended compensating technique raises the system's power quality by utilizing the wholly DC energy storage and the active power sharing across UPQC converters. The DVR and DSTATCOM compensators do not include these features. The THD of the fuzzy controller improved the UPQC controller. The simulation's outcomes explain that it is possible to regulate the

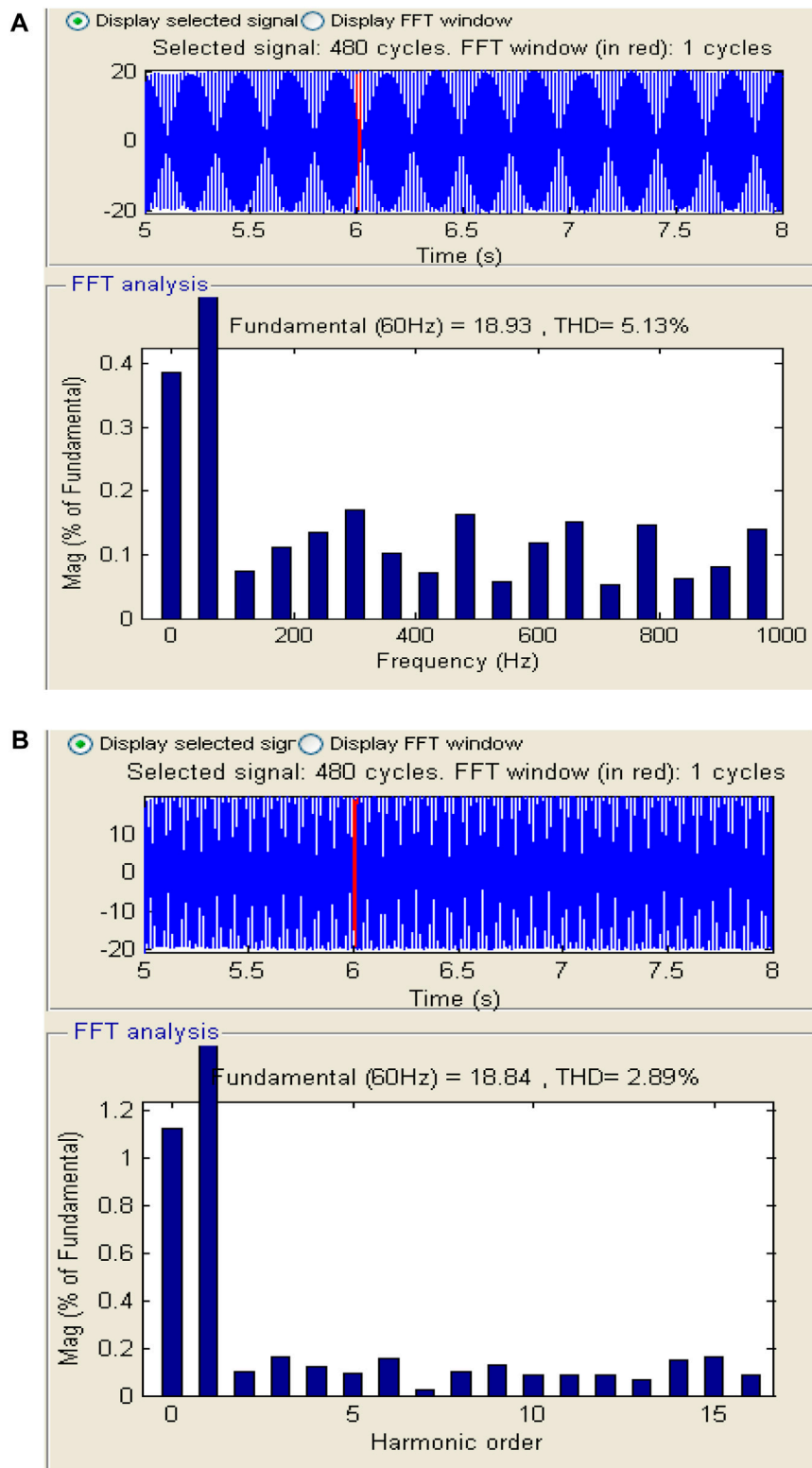


FIGURE 22 (A) FFT analysis with UPQC controller and (B) FFT analysis with fuzzy controller.

voltage induced by an unexpected load connection and reject the power fluctuations caused by the “tower shadow effect” with satisfactory results. The research example thus shows that the

suggested compensation scheme accomplishes its objectives. The performance levels of the various types of compensators will be compared in future research.

Data availability statement

The original contributions presented in the study are included in the article/Supplementary material, further inquiries can be directed to the corresponding authors.

Author contributions

MP: Conceptualization, Data curation, Formal Analysis, Funding acquisition, Investigation, Methodology, Project administration, Resources, Software, Supervision, Validation, Visualization, Writing–original draft, Writing–review and editing. KG: Conceptualization, Data curation, Formal Analysis, Funding acquisition, Investigation, Methodology, Project administration, Resources, Software, Supervision, Validation, Visualization, Writing–original draft, Writing–review and editing. BS: Conceptualization, Data curation, Formal Analysis, Funding acquisition, Investigation, Methodology, Project administration, Resources, Software, Supervision, Validation, Visualization, Writing–original draft, Writing–review and editing. MK: Conceptualization, Data curation, Formal Analysis, Funding acquisition, Investigation, Methodology, Project administration, Resources, Software, Supervision, Validation, Visualization, Writing–original draft, Writing–review and editing. CR: Conceptualization, Data curation, Formal Analysis, Funding acquisition, Investigation, Methodology, Project administration, Resources, Software, Supervision, Validation, Visualization, Writing–original draft, Writing–review and editing. HK: Conceptualization, Data curation, Formal Analysis, Funding acquisition, Investigation, Methodology, Project administration, Resources, Software, Supervision, Validation, Visualization,

Writing–original draft, Writing–review and editing. KA: Software, Supervision, Validation, Visualization, Writing–original draft, Writing–review and editing, Conceptualization, Data curation, Formal Analysis, Funding acquisition, Investigation, Methodology, Project administration, Resources. AY: Conceptualization, Data curation, Formal Analysis, Funding acquisition, Investigation, Methodology, Project administration, Resources, Software, Supervision, Validation, Visualization, Writing–original draft, Writing–review and editing.

Funding

The author(s) declare that no financial support was received for the research, authorship, and/or publication of this article.

Conflict of interest

The authors declare that the research was conducted in the absence of any commercial or financial relationships that could be construed as a potential conflict of interest.

Publisher's note

All claims expressed in this article are solely those of the authors and do not necessarily represent those of their affiliated organizations, or those of the publisher, the editors and the reviewers. Any product that may be evaluated in this article, or claim that may be made by its manufacturer, is not guaranteed or endorsed by the publisher.

References

- Chen, C., Wu, X., Yuan, X., and Zheng, X. (2022). A new technique for the subdomain method in predicting electromagnetic performance of surface-mounted permanent magnet motors with shaped magnets and a quasi-regular polygon rotor core. *IEEE Trans. Energy Conversion* 38, 1396–1409. doi:10.1109/TEC.2022.3217042
- Chishti, F., Murshid, S., and Singh, B. (2020). Weak grid inertia WEGS with hybrid generalized integrator for power quality improvement. *IEEE Trans. Ind. Electron.* 67 (2), 1113–1123. doi:10.1109/TIE.2019.2898598
- Damchi, Y., and Eivazi, A. (2022). Power swing and fault detection in the presence of wind farms using generator speed zero-crossing moment. *Int. Trans. Electr. Energy Syst.* 2022, 1–17. doi:10.1155/2022/2569810
- Duan, Y., Zhao, Y., and Hu, J. (2023). An initialization-free distributed algorithm for dynamic economic dispatch problems in microgrid: modeling, optimization and analysis. *Sustain. Energy, Grids Netw.* 34, 101004. doi:10.1016/j.segan.2023.101004
- Hao, Y., Liang, J., Wang, K., Wu, G., Joseph, T., and Sun, R. (2020). Influence of active power output and control parameters of full-converter wind farms on sub-synchronous oscillation characteristics in weak grids. *Energies* 12, 1–17. doi:10.3390/en13195225
- Huang, N., Chen, Q., Cai, G., Xu, D., Zhang, L., and Zhao, W. (2021). Fault diagnosis of bearing in wind turbine gearbox under actual operating conditions driven by limited data with noise labels. *IEEE Trans. Instrum. Meas.* 70, 1–10. doi:10.1109/TIM.2020.3025396
- Li, P., Hu, J., Qiu, L., Zhao, Y., and Ghosh, B. K. (2022b). A distributed economic dispatch strategy for power–water networks. *IEEE Trans. Control Netw. Syst.* 9 (1), 356–366. doi:10.1109/TCNS.2021.3104103
- Li, S., Zhao, X., Liang, W., Hossain, M. T., and Zhang, Z. (2022a). A fast and accurate calculation method of line breaking power flow based on Taylor expansion. *Front. Energy Res.* 10. doi:10.3389/fenrg.2022.943946
- Lin, L., Zhang, J., Gao, X., Shi, J., Chen, C., and Huang, N. (2023). Power fingerprint identification based on the improved V-I trajectory with color encoding and transferred CBAM-ResNet. *PLoS one* 18 (2), e0281482. doi:10.1371/journal.pone.0281482
- Liu, H., Wang, W., Cui, J., and Tang, F. (2018). Optimal power factor regulation of dispersed wind farms under diverse load and stochastic wind conditions based on improved firefly algorithm. *Math. Probl. Eng.* 2018, 1–11. doi:10.1155/2018/6203278
- Liu, Y., Liu, X., Li, X., Yuan, H., and Xue, Y. (2023). Model predictive control-based dual-mode operation of an energy-stored quasi-Z-source photovoltaic power system. *IEEE Trans. Industrial Electron.* 70 (9), 9169–9180. doi:10.1109/TIE.2022.3215451
- Lu, L., Wu, W., Gao, Y., Pan, C., Yu, X., Zhang, C., et al. (2022). Study on current discrepancy and redistribution of HTS non-insulation closed-loop coils during charging/discharging and subsequent transient process toward steady-state operation. *Supercond. Sci. Technol.* 35 (9), 095001. doi:10.1088/1361-6668/ac7dfc
- Miaofen, L., Youmin, L., Tianyang, W., Fulei, C., and Zhike, P. (2023). Adaptive synchronous demodulation transform with application to analyzing multicomponent signals for machinery fault diagnostics. *Mech. Syst. Signal Process.* 191, 110208. doi:10.1016/j.ymssp.2023.110208
- Morgan, M. Y., El-Deib, A. A., and El-Marsafawy, M. (2018). Wind farm dynamic models assessment under weak grid conditions. *IET Renew. Power Gener.* 12 (12), 1325–1334. doi:10.1049/iet-rpg.2017.0292
- Nie, Y., Wang, H., Gao, L., Wu, C., and Xi, M. (2022). Adaptive parameter estimation for static var generators based on wind speed fluctuation of wind farms. *Int. Trans. Electr. Energy Syst.* 2022, 1–12. doi:10.1155/2022/3877777
- Raju, K. G., and Rao, K. V. G., "Fuzzy – genetic algorithm approach for fact placement in electrical power system," no. 1, pp. 17, 2015.
- Rao, K. V. G., Kiran Kumar, M., and Srikanth Goud, B. (2023). An independently controlled two output half bridge resonant LED driver. *Electr. Power Components Syst.* 0 (0), 1–21. doi:10.1080/15325008.2023.2238695
- Ray, P., Ray, P. K., and Kumar Dash, S. (2021). Power quality enhancement and power flow analysis of a PV integrated UPQC system in a distribution network. *IEEE Trans. Industry Appl.* 58 (1), 201–211. doi:10.1109/tia.2021.3131404

- Sang, S., Zhang, C., Cai, X., Molinas, M., Zhang, J., and Rao, F. (2019). Control of a type-IV wind turbine with the capability of robust grid-synchronization and inertial response for weak grid stable operation. *IEEE Access* 7, 58553–58569. doi:10.1109/ACCESS.2019.2914334
- Shirkhani, M., Tavooosi, J., Danyali, S., Sarvenoe, A. K., Abdali, A., Mohammadzadeh, A., et al. (2023). A review on microgrid decentralized energy/voltage control structures and methods. *Energy Rep.* 10, 368–380. doi:10.1016/j.egy.2023.06.022
- Song, J., Mingotti, A., Zhang, J., Peretto, L., and Wen, H. (2022a). Fast iterative-interpolated DFT phasor estimator considering out-of-band interference. *IEEE Trans. Instrum. Meas.* 71, 1–14. doi:10.1109/TIM.2022.3203459
- Song, J., Mingotti, A., Zhang, J., Peretto, L., and Wen, H. (2022b). Accurate damping factor and frequency estimation for damped real-valued sinusoidal signals. *IEEE Trans. Instrum. Meas.* 71, 1–4. doi:10.1109/TIM.2022.3220300
- Song, X., Wang, H., Ma, X., Yuan, X., and Wu, X. (2023). Robust model predictive current control for a nine-phase open-end winding PMSM with high computational efficiency. *IEEE Trans. Power Electron.* 38 (11), 13933–13943. doi:10.1109/TPEL.2023.3309308
- Srikanth, G., Venkata Sai Kalyani, T., Venkata Govardhan Rao, K., and Sanjeev, G. (2023). Amalgamation of smart grid with renewable energy sources. *International J. of Smart Grid-ijSmartGrid* 7 (2), 103–107. doi:10.20508/ijsmartgrid.v7i2.289.g276
- Sun, Q., Lyu, G., Liu, X., Niu, F., and Gan, C. (2023). Virtual current compensation-based quasi-sinusoidal-wave excitation scheme for switched reluctance motor drives. *IEEE Trans. Industrial Electron.*, 1–11. doi:10.1109/TIE.2023.3333056
- Venkata Govardhan Rao, K., Kumar, M. K., Goud, B. S., Bajaj, M., Abou Houran, M., and Kamel, S. (2022). Design of a bidirectional DC/DC converter for a hybrid electric drive system with dual-battery storing energy. *Front. Energy Res.* 10 (November), 1–19. doi:10.3389/fenrg.2022.972089
- Wang, H., Wang, B., Luo, P., Ma, F., Zhou, Y., and Mohamed, M. A. (2022b). State evaluation based on feature identification of measurement data: for resilient power system. *CSEE J. Power Energy Syst.* 8 (4), 983–992. doi:10.17775/CSEEJPES.2021.01270
- Wang, Y., Chen, P., Yong, J., Xu, W., Xu, S., and Liu, K. (2022a). A comprehensive investigation on the selection of high-pass harmonic filters. *IEEE Trans. Power Deliv.* 37 (5), 4212–4226. doi:10.1109/TPWRD.2022.3147835
- Wang, Y., Xia, F., Wang, Y., and Xiao, X. (2023). Harmonic transfer function based single-input single-output impedance modeling of LCCHVDC systems. *J. Mod. Power Syst. Clean Energy.* doi:10.35833/MPCE.2023.000093
- Xiao, S., Wang, Z., Wu, G., Guo, Y., Gao, G., Zhang, X., et al. (2023). Critical assessment of the delivery methods of chemical and natural postharvest preservatives for fruits and vegetables: a review. *IEEE Trans. Transp. Electrification.* 1–23. doi:10.1080/10408398.2023.2289071
- Xie, X., and Sun, Y. (2022). A piecewise probabilistic harmonic power flow approach in unbalanced residential distribution systems. *Int. J. Electr. Power and Energy Syst.* 141, 108114. doi:10.1016/j.ijepes.2022.108114
- Yan, C., Yao, W., Wen, J., Fang, J., Ai, X., and Wen, J. (2020). Modelling and comparison analysis of grid-connected DFIG-based wind farm in weak grid. *IET Renew. Power Gener.* 14 (13), 2406–2415. doi:10.1049/iet-rpg.2019.1382
- Yang, C., Wu, Z., Li, X., and Fars, A. (2024). Risk-constrained stochastic scheduling for energy hub: integrating renewables, demand response, and electric vehicles. *Energy* 288, 129680. doi:10.1016/j.energy.2023.129680
- Yang, J., Zhang, R., Sun, Q., and Zhang, H. (2015). Optimal wind turbines micro-siting in onshore wind farms using fuzzy genetic algorithm. *Math. Probl. Eng.* 2015, 1–9. doi:10.1155/2015/324203
- Yang, Y., Zhang, Z., Zhou, Y., Wang, C., and Zhu, H. (2023). Design of a simultaneous information and power transfer system based on a modulating feature of magnetron. *IEEE Trans. Microw. Theory Tech.* 71 (2), 907–915. doi:10.1109/TMTT.2022.3205612
- Yuan, S., Hao, Z., Zhang, T., Yuan, X., and Shu, J. (2019). Impedance modeling based method for sub/supersynchronous oscillation analysis of D-PMSG wind farm. *Appl. Sci.* 2813, 1–16. doi:10.3390/app9142831
- Zhang, X., Gong, L., Zhao, X., Li, R., Yang, L., and Wang, B. (2023). Voltage and frequency stabilization control strategy of virtual synchronous generator based on small signal model. *Energy Rep.* 9, 583–590. doi:10.1016/j.egy.2023.03.071
- Zhu, L., Li, Z., and Hou, K. (2022). Effect of radical scavenger on electrical tree in cross-linked polyethylene with large harmonic superimposed DC voltage. *High. Volt.* 8, 739–748. doi:10.1049/hve2.12302

Nomenclature

WF	Wind Form	WPPs	Wind Power Plants
SCIG	Squirrel Cage Induction Generator	SCR	Short Circuit Ratio
MV	Medium Voltage	STATCOM	Synchronous Compensator
PCC	Point of Common Coupling	BESS	Battery Energy Storage System
PQ	Power Quality	VSG	Virtual Synchronous Generator
CUPS	Custom Power Devices	LVRT	Low-Voltage Ride Through
UPQC	Unified Power Quality Compensator	PLL	Phase Locked Loop
DC	Direct Current	WEGS	Wind Energy Generating System
THD	Total Harmonic Distortion	MSVSC	machine-side voltage source converter
PI	Proportional Integral	UGVSC	Utility Grid Side Voltage Source Converter
HV	High Voltage	SG	Synchronous Generator
WG	Weak Grid	D-PMSG	Direct-Drive Permanent Magnet Synchronous Generators
FACTS	Flexible AC Transmission System	FAM	Fully Aggregated Mode
QZSIMC	Quasi Z-Source Indirect Matrix Converter		
PMG	Permanent Magnetic Generator		
DDWECS	Direct Drive Wind Energy Conversion Systems		
S-ANNC	Soccer League Algorithm trained Artificial Neural Network Controller		
STF	Self Tuning Filter		
UVGM	Unit Vector Generation Method		
PWM	Pulse Width Modulation		
VSI	Voltage Source Inverter		
CSI	Current Source Inverter		
PJLL	Phase Locked Loop		
LVRT	Low Voltage Ride Through		
DSTATCOM	Distribution Static Synchronous Compensator		
errA	Error Signal		
RerrA	Error Rate Signal		
PU	Per Unit		
FLC	Fuzzy Logic Controller		
DFIG	Doubly-Fed Induction Generator		
SSO	Sub-Synchronous Oscillation		
WFCM	Weighted Fuzzy C-Means		
OEM	Orthogonal Experiment Method		
V_{synC}	Virtual Synchronous Control		
WTs	Wind Turbines		
VSC-HVDC	Voltage Source Converter-Based HVDC		
SEC	Sending-End Converter		
PMSG	Permanent Magnet Synchronous Generators		
SSR	Sub Synchronous Resonance		
LCC HVDC	line-commutated converter-based high-voltage direct-current		